Joseph Chen
Department of Biomedical Engineering,
Vanderbilt University,
2213 Garland Avenue,
Nashville, TN 37232-0493
e-mail: joseph.chen@vanderbilt.edu

Jon R. Peacock
Department of Biomedical Engineering,
Vanderbilt University,
2213 Garland Avenue,
Nashville, TN 37232-0493
e-mail: jon.r.peacock@vanderbilt.edu

Janelle Branch
Department of Civil
and Environmental Engineering,
Vanderbilt University,
400 24th Avenue South,
Nashville, TN 37212
e-mail: janelle.l.branch@vanderbilt.edu

W. David Merryman
Department of Biomedical Engineering,
Vanderbilt University,
2213 Garland Avenue,
Nashville, TN 37232-0493
e-mail: david.merryman@vanderbilt.edu

Biophysical Analysis of Dystrophic and Osteogenic Models of Valvular Calcification

Calcific aortic valve disease (CAVD) is a significant cardiovascular disorder characterized by the formation of calcific nodules (CN) on the valve. In vitro assays studying the formation of these nodules were developed and have led to many significant mechanistic findings; however, the biophysical properties of CNs have not been clearly defined. A thorough analysis of dystrophic and osteogenic nodules utilizing scanning electron microscopy (SEM), energy dispersive spectrometry (EDS), and atomic force microscopy (AFM) was conducted to describe calcific nodule properties and provide a link between calcific nodule morphogenesis in vitro and in vivo. Unique nodule properties were observed for dystrophic and osteogenic nodules, highlighting the distinct mechanisms occurring in valvular calcification. [DOI: 10.1115/1.4029115]

Introduction

The pathogenesis of CAVD involves the deposition of calcium rich nodules on the fibrosa layer of aortic valve leaflets [1–3]. The presence of these structures significantly impedes proper opening and closing of the valve, leading to left ventricular pressure overloading and eventual heart failure [2,4]. Two major types of valvular calcification have been observed in diseased excised tissue: dystrophic and osteogenic [5]. Dystrophic calcification is the predominant form of valvular calcification being found in 83% of diseased valves and is described as an amorphous crystalline material [6]. Osteogenic calcification is present in 13% of valves containing dystrophic calcification and is identified by the presence of osteoid matrix reminiscent of active bone formation [6]. At present, there exists only surgical intervention for CAVD, which although effective, includes a 3% mortality rate and is only utilized at the end stage disease [7,8]. Efforts to describe the mechanisms of valvular calcification may lead to the development of novel pharmacological treatments for CAVD [9–11].

The etiology of CAVD has been extensively studied through the development of valvular calcification in vitro models [5,10,12–22]. These models describe the formation of CNs via aortic valve interstitial cells (AVICs) in unique culture conditions and are thought to mimic the dystrophic and osteogenic calcification found in diseased explanted aortic valve leaflets [5,6]. The CNs generated from each model appear morphologically similar in that they are cellular aggregates but form via distinct mechanisms and have unique features. Dystrophic nodules form on stiff substrates, are characterized by cell death, and involve the differentiation of quiescent AVICs into activated myofibroblasts via inflammatory cytokines such as TGF-β1 [14,15,23,24]. Conversely, osteogenic nodules form on compliant substrates through the active secretion of bone matrix via osteogenic AVICs [5,13,25]. These in vitro systems have helped identify many important mediators of dystrophic and osteogenic calcification; however, there exists ambiguity regarding what distinguishes each type of CNs [26]. The physicochemical composition and biophysical properties of the two nodule types remain largely undefined and their relationship to in vivo valvular calcification is unclear [13]. Clarifying the properties of CNs is necessary to more clearly delineate the two nodule types and provide a correlation between mechanistic changes and biophysical properties.

Few studies have been conducted to describe the physicochemical properties of CNs. Cloyd et al. examined CNs formed using calcifying media supplemented with TGF-β1 with techniques such as SEM, transmission electron microscopy (TEM), and Raman spectroscopy [26]. Strikingly, these CNs were not mineralized but rather were rich in collagen content indicative of myofibroblast remodeling. This is in contrast to a study demonstrating, via TEM, that CNs formed in calcifying media without TGF-β1 contained a mineralized core [27]. Additionally, a seminal study investigating CN formation using infrared spectroscopy revealed that the CNs formed with TGF-β1 treatment exhibited a spectrum corresponding to the presence of hydroxyapatite in the nodule center [16]. Taken together, these studies suggest that all CNs are not equal and their properties are highly dependent on their culture conditions. Furthermore, these contrasting findings highlight the uncertainty that exists regarding CN properties and necessitate additional studies evaluating the physicochemical and biophysical properties of dystrophic and osteogenic CNs.

In this study, we utilize SEM coupled with X-ray EDS (SEM-EDS) and AFM to define CN characteristics through two published in vitro systems of dystrophic and osteogenic calcification [13,19]. We found that both nodule types contained Ca and P contents; however, the regions where calcification forms were dramatically different. Dystrophic nodules had little to no surface calcification, whereas osteogenic nodules had an abundance of calcified spheres on the surface similar to what has been observed

Manuscript received August 25, 2014; final manuscript received November 13, 2014; published online January 26, 2015. Editor: Victor H. Barocas.

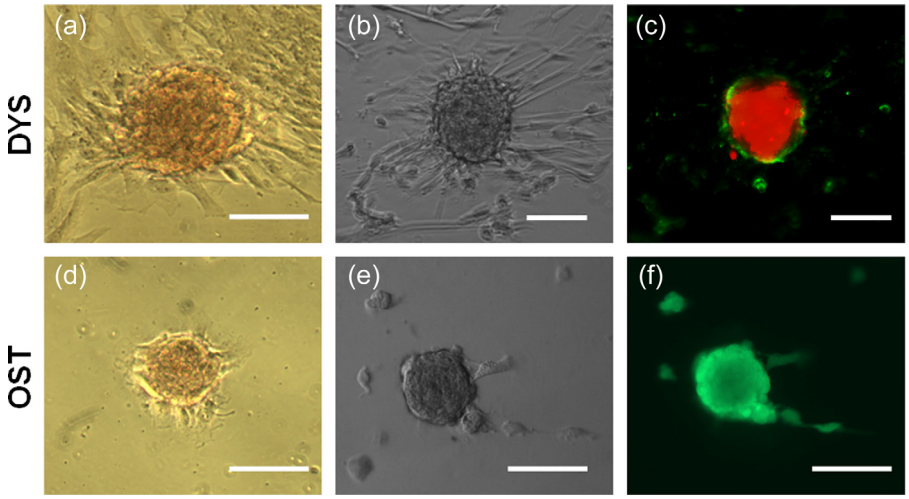

Fig. 1 Dystrophic and osteogenic CNs exhibit differences in morphology and cell viability. (*a*) and (*d*) Dystrophic CNs and Osteogenic CNs stain positive for Alizarin Red. (*b*) and (*e*) Bright field images reveal morphological differences between dystrophic and osteogenic nodules. (*c*) Annexin/PI stain show strong uptake of PI stain in the nodule center with an Annexin V positive ring around dystrophic nodules while Calcein AM/PI stain show living cells within the osteogenic nodules and no uptake of PI stain. Scalebar = 100 μm.

in vivo [28]. Also, both nodules had regions that did not contain calcification and exhibited modulus readings similar to that of cells. These data reveal a heterogeneous makeup of both nodules that have not been previously described. Furthermore, characteristics specific to dystrophic and osteogenic types were identified. Collectively, these findings ascribe unique characteristics to CN types and provide evidence connecting in vitro and in vivo valvular calcification.

Methods

AVIC Isolation and Culture. Porcine aortic valve leaflets were excised from sacrificed animals within 10 min of slaughter at a local abattoir. Leaflets were stored in phosphate buffered saline (PBS) with 1% penicillin/streptomycin (Cellgro; Manassas, VA) at 4 °C to ensure survival. Within 3 h of sacrifice, AVICs were isolated as previously described [29]. Briefly, after the removal of the endothelium, the leaflet was diced and digested in a 2 mg/ml collagenase solution (Worthington Biochemical Corp., Lackwood, NJ) for 1 h at 37 °C and 5% CO_2. The collagenase solution with the tissue was passed through a cell strainer to collect a cell solution, which was centrifuged at 1500 RPM for 10 min to obtain the cell pellet. The pellet was then resuspended in Dulbecco's modified eagle medium (DMEM) supplemented with 10% fetal bovine serum (FBS) (Atlanta Biologicals, Lawrenceville, GA) and 1% penicillin/streptomycin antibiotic. Cells were either cryopreserved at passage 0 to preserve a quiescent phenotype or seeded on tissue culture dishes and incubated at 37 °C and 5% CO_2 with media changes every three days [30].

Calcific Nodule Assays. Dystrophic and osteogenic CNs were generated according to published in vitro systems [5,13,19,20]. For dystrophic CN formation, AVICs were cultured on BioFlex Pronectin culture plates (Flexcell International Corporation, Hillsborough, NC) at 6×10^4 cells/cm^2 in normal growth media and were given a day to reach confluence. After AVIC confluence, normal growth media were removed and replaced with growth media supplemented with 5 ng/ml porcine TGF- β1 (R&D Systems, Minneapolis, MN) for 24 h. The plates were then subject to equibiaxial strain via the Flexcell-4000 Tension System at a strain magnitude of 15% and a frequency of 0.75 Hz for 24 h.

Osteogenic CNs were developed on 24 kPa polyacrylamide hydrogels fabricated as previously described [13,31,32]. Briefly, amino-silanated coverslips were prepared and utilized as a surface for hydrogel polymerization. 24 kPa hydrogels (10% acrylamide and 0.225% bis-acrylamide) were produced via free radical polymerization and functionalization was performed via Sulfo-SANPAH conjugation of 10 μg/ml fibronectin to the polyacrylamide substrate. P0 AVICs were plated onto the hydrogels at a density of 1×10^4 cells/cm^2 and allowed to attach overnight. Cells were then treated with osteogenic media consisting of DMEM supplemented with 10% FBS, 1% penicillin/streptomycin antibiotic, 10 mM β-glycerophosphate, 10 μg/ml ascorbic acid, and 10 nM dexamethasone for 6 days.

Calcific Nodule Staining and Analysis. CNs were assayed for calcium deposition using the Alizarin red stain [33]. CNs were rinsed with three times with PBS, fixed with 3.7% neutral buffered formaldehyde for 15 min, and rinsed again with PBS. For microscopic analysis, 1 mL of 14 mM Alizarin red solution was added to AVIC cultures for 30 min. After staining, the wells were washed with de-ionized water (dH_2O) to remove excess dye. Positively stained nodules were determined by visible red color.

To confirm cell viability properties in each calcific nodule type, Annexin V/propidium iodide (PI) and Calcein AM/PI stains were utilized. Dystrophic nodules were rinsed with PBS and stained with Annexin V conjugated with Alexa fluor 488 (5% solution in Annexin binding buffer; Invitrogen) for 15 min to detect apoptotic cells. Propidium iodide (0.4% solution in Annexin binding buffer; Invitrogen) was used as a counterstain for necrotic cells. Osteogenic nodules were rinsed in PBS and stained with fluorescently labeled Calcein AM (0.3% solution in PBS) to detect living cells and PI (0.3% solution in PBS) to detect dead cells. Images were taken with a Nikon TE300 inverted tissue culture fluorescence microscope.

SEM and X-Ray EDS. For SEM-EDS analysis, CN samples were fixed in 2.5% gluteraldehyde in 0.1 M sodium cacodylate buffer solution for 1 h at room temperature and 24 h at 4 °C. Samples were subsequently washed three times with sodium cacodylate buffer. CNs were then dehydrated by a series of ethanol washes (30%, 50%, 70%, and 95% ethanol) for 15 min each. Dehydration was completed with two 15 min washes with 100% ethanol. Samples underwent critical point drying and were then placed on carbon tape mounted on aluminum stubs. Silver paint

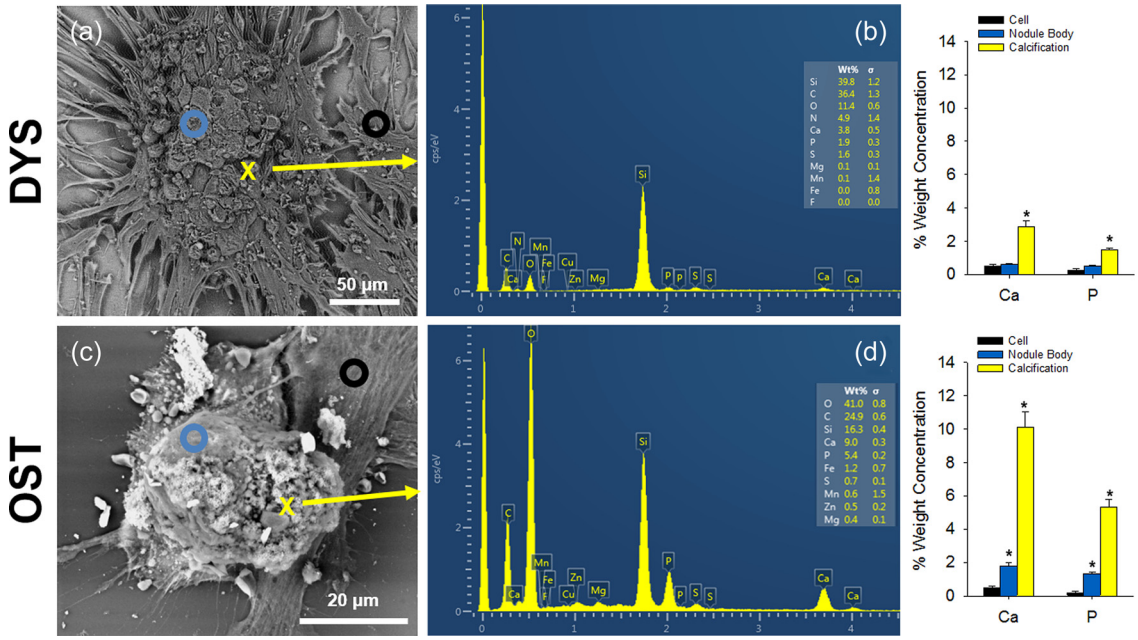

Fig. 2 EDS reveals significant Ca and P content in CNs. (*a*) and (*d*) Backscattered SEM image of CNs with annotations showing regions of the nodules scanned with EDS. A black circle represents an EDS scan on cells; a blue circle represents an EDS scan on the nodule body; and a yellow X marks a point scanned to represent an area of calcification. (*b*) Representative EDS spectrum of a dystrophic nodule scanned at the yellow X in A. Ca and P scans show a weight percent of 2.8 and 1.5, respectively. (*c*) Relative percent weight concentration shows significantly higher amounts of Ca and P in regions of calcification. (*e*) Representative EDS spectrum of an osteogenic nodule scanned at the yellow X in D shows a weight percent of 10.1 and 5.3 for Ca and P, respectively. (*f*) Relative percent weight concentration shows dramatically higher levels of Ca and P in calcification regions. * indicates $p \leq 0.05$

was applied on the carbon tape to reduce charging effects, and the samples were scanned in environmental SEM (ESEM) mode.

A Phillips/FEI Quanta 650 field emission electron microscope with ESEM capability and equipped with an Oxford Instruments X-Max 50 mm^2 silicon drift detector (SDD) and was used to collect backscattered images and semiquantitative chemical data of representative nodules and cells from the osteogenic and dystrophic samples. EDS spectra were generated on > 3 nodules of each nodule type with > 5 scans per nodule. The SEM was operated in ESEM mode at 130 Pa to avoid carbon coating and to reduce sample charging. A spot size of 3.5, a working distance of 10 mm, and a voltage of 10 keV were used to collect all backscattered electron SEM images and EDS data. A voltage of 10 keV was chosen because it has sufficient energy to exceed the critical excitation energy of the Ca K shell (3.6905 keV). A beam measurement of 200,000 counts was performed on a titanium standard prior to collecting EDS data. Point spectra were collected for 60 s, which corresponded to $> 80{,}000$ area counts. All EDS data were populated in the OXFORD AZTEC software, and the Aztec default standards were applied during the postprocessing quantitative analysis.

AFM. AFM data and corresponding bright-field images were captured with a Catalyst Bioscope AFM (Bruker AXS, Madison, WI) and a nonconductive silicon nitride cantilever with a blunted pyramidal tip ($f_0 = 15$ kHz, $k = 0.03$ N/m) suitable for biological samples was used for all measurements. The AFM was calibrated each day in fluid using a relative calibration method as previously described [34]. Briefly, the AFM was operated in peak force quantitative nanomechanical mapping mode, and deflection sensitivity was measured on a glass slide. The cantilever spring constant was calculated using the thermal tune method built in to the AFM software. Three to six $15 \times 15\ \mu$m area scans were taken on a Bruker-provided poly(dimethyl siloxane) calibration standard ($E = 2.5$ MPa) in order to adjust peak force set-point and amplitude, as well as tip radius. These parameters were kept constant after calibration. Scans of samples ranged from $5 \times 5\ \mu$m to $30 \times 30\ \mu$m in area.

For all experiments, live nonfixed samples were scanned to prevent potential artifacts due to fixation. Three cells or nodules were scanned with three different regions scanned for each. Median modulus values for each region were determined from the modulus distribution and a single median modulus value was calculated for each cell or nodule by averaging the three regional median modulus values. Median stiffness values for the AVICs ($n = 3$) and CNs ($n = 3$) were then calculated as the mean ± SEM

Statistical Analyses. The data are reported as the mean of all replicates, and error is given as standard error of the mean. Statistical significance between treatments was determined by one-way ANOVA and Holm-Sidek tests.

Results

Dystrophic and Osteogenic CNs Exhibit Differences in Morphology and Cell Viability. CN formation via dystrophic and osteogenic culture systems generated distinct CNs consistent with previous findings [13,19]. Bright field images reveal morphological differences with dystrophic nodules exhibiting aggregates with elongated cells in a radial pattern along the periphery of the nodule (Figs. 1(*a*) and 1(*b*)) and osteogenic nodules having flattened cells lining regions of the aggregate (Figs. 1(*d*) and 1(*e*)). Additionally, dystrophic nodules were generally larger than osteogenic CNs. Using the calcium stain Alizarin red, both dystrophic and osteogenic CNs stained positively in the nodule center (Figs. 1(*a*) and 1(*b*)). Stains for cell viability were conducted on both nodule types to confirm the cell death mediated and active bone forming calcification of dystrophic and osteogenic systems, respectively. Annexin V/PI stain on dystrophic nodules revealed an intensely stained necrotic core with Annexin V positive apoptotic cells lining the periphery of the CN (Fig. 1(*c*)). Conversely, Calcein

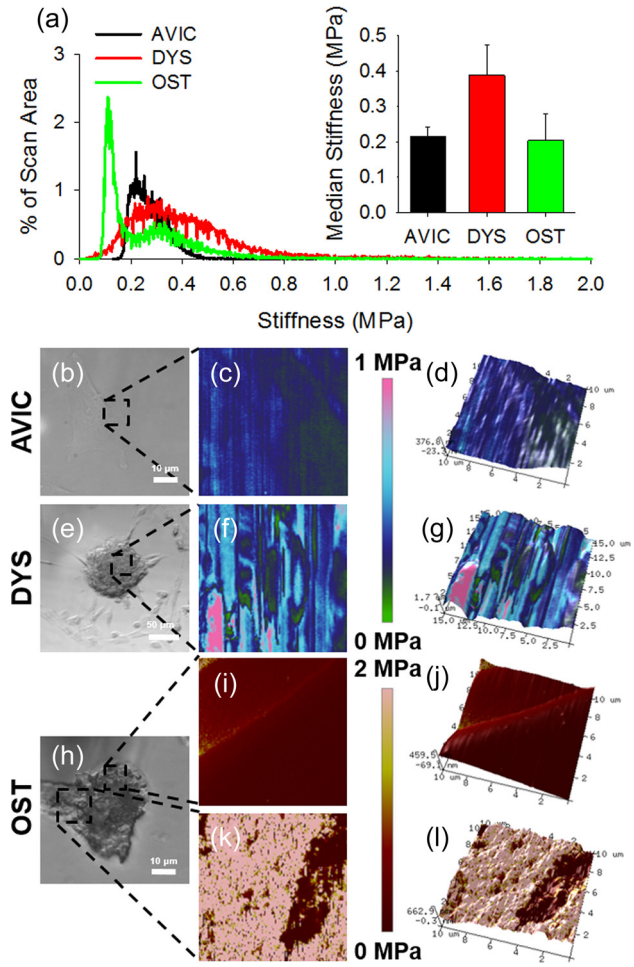

Fig. 3 ***Biomechanical analysis reveals nodule heterogeneity.*** **(*a*) Representative modulus scan distributions for cells and nodules. Inset graph shows average median modulus and reveals no significant difference between sample groups; however, osteogenic nodules had bimodal distribution, which likely skews downward their overall stiffness. (*b*), (*e*), and (*h*) Regions scanned on AVIC, dystrophic, and osteogenic nodules via AFM are represented by the black dotted box. AVIC and osteogenic nodule body scans display consistent homogeneous modulus scans (*c*) and (*i*) while dystrophic nodules exhibit heterogeneous modulus scans (*f*). Osteogenic nodules contain dramatically stiffer regions resembling spherical calcifications on the surface of the nodule body revealing the heterogeneous make up of osteogenic nodules. (*d*), (*g*), (*j*), and (*l*) 3D topographical maps for AVIC, dystrophic, and osteogenic nodules were overlaid with the modulus map.**

AM/PI staining of osteogenic nodules showed no uptake of PI stain but an incorporation of Calcein AM stain confirming the presence of living cells within the nodule (Fig. 1(*f*)).

EDS Analysis Reveal Significant Ca and P Content in CNs. EDS spectra were collected from three regions on each nodule sample: cell, nodule body, and calcification. Regions were identified via backscattered electron SEM images and EDS mapping of the nodules (data not shown). Furthermore, distinct differences in surface topography were confirmed by secondary electron imaging between the nodule types with dystrophic nodules exhibiting rounded cellular structures across the surface of the nodule and osteogenic nodules having smooth regions in addition to spherical materials on the surface (Figs. 2(*a*) and 2(*d*)).

Spectra from dystrophic nodules reveal average percent weight concentrations of 0.52 ± 0.08 and 0.26 ± 0.10, 0.62 ± 0.03 and 0.53 ± 0.04, and 2.88 ± 0.34 and 1.48 ± 0.12 for Ca and P from cell, nodule body, and calcification regions, respectively (Figs. 2(*b*) and 2(*c*)). Ca and P concentrations in calcification regions were significantly higher than those in the nodule body and the cell. Although the percent weight concentration was higher, calcification areas in the dystrophic nodule were scarce and often found in regions that were deeper within the nodule and not at the surface. Spectra from osteogenic nodules show average percent weight concentrations of 0.51 ± 0.09 and 0.16 ± 0.01, 1.78 ± 0.21 and 1.33 ± 0.10, and 10.09 ± 0.90 and 5.31 ± 0.49 for Ca and P from cell, nodule body, and calcification regions, respectively (Figs. 2(*e*) and 2(*f*)). Osteogenic nodule spectra show dramatically higher levels of Ca and P in spherical materials on the surface of the nodule compared to the nodule body and cells. Additionally, Ca and P concentrations from the osteogenic nodule body were also higher than that of cells. Interestingly, osteogenic calcification possessed a higher concentration of Ca and P than dystrophic calcification.

Biomechanical Analysis Reveals Nodule Heterogeneity. AFM scans of live cells, dystrophic nodules, and osteogenic nodules provide a wide distribution of modulus values that we represent by taking the averaged median value for each cell or CN after multiple successful scans. Averaged modulus median values of 220 kPa, 390 kPa, and 200 kPa were noted for cells, dystrophic nodules, and osteogenic nodules, respectively (Fig. 3(*a*)). No significant differences in modulus were found between the cell and CN groups suggesting that the nodule surfaces are comprised mostly of cellular material. Live AVICs scans revealed largely homogeneous modulus properties, while certain regions of the osteogenic nodule body were similarly homogeneous (Figs. 3(*c*), 3(*d*), 3(*i*), and 3(*j*)). However, osteogenic CN heterogeneity was noted as areas of the osteogenic nodule surface also contained significantly stiffer calcified spheres that were discernable via AFM (Figs. 3(*k*) and 3(*l*)). Dystrophic calcification scans indicated a more variable modulus map corresponding to changes in topography, but the modulus values were not significantly different than that of AVICs and osteogenic nodules (Figs. 3(*f*) and 3(*g*)).

Discussion

Since the seminal study describing CNs, much research has been conducted to evaluate the molecular processes that mediate the formation and evolution of these nodules [16]. However, there has been a lack of clarity regarding the intrinsic physicochemical and biophysical properties of the CNs formed in vitro. Characterization of these properties is necessary to provide the link between in vitro CN formation and in vivo valvular calcification and strengthen the impact of the findings from these in vitro systems. Additionally, the perception of CN formation has changed drastically in recent years from an understanding of one nodule expressing both dystrophic and osteogenic properties to distinct dystrophic and osteogenic nodules with specific properties [5,13–16]. Defining dystrophic and osteogenic nodule properties will help delineate characteristics unique to each nodule type and may provide important correlations between mechanistic information and biophysical properties. In this study, we sought to define the physicochemical and biophysical properties of dystrophic and osteogenic CNs formed via published in vitro systems.

Dystrophic and osteogenic CNs generated in this study were assessed to ensure that they generated distinct nodules that corresponded with previous findings [13,19]. Dystrophic nodules were formed via TGF-β1 activation of AVICs under a 15% mechanical strain environment for 24 h. These nodules contained a necrotic core with a ring of apoptotic cells surrounding the nodule periphery as revealed by Annexin V/PI stain. Osteogenic nodules formed after six days in calcifying media on compliant PA gels of 24 kPa. The whole nodule body stained positively for Calcein AM with no uptake of PI stain indicating viable cells. Both nodules also stained positively for Alizarin red, a calcium stain. These results

confirm that two unique nodule types consistent with dystrophic and osteogenic calcification were formed.

Backscattered electron SEM images revealed dramatic differences in nodule chemical composition. Dystrophic nodules were comprised of round structures that covered the nodule body and were presumably dead cell bodies due to their uptake of PI. In addition, the backscattered images were fairly similar in brightness, indicating similar physicochemical properties throughout the surface of the dystrophic nodule. Conversely, osteogenic nodules exhibited smooth regions in the nodule body with small spherical materials covering regions of the nodule body. These spherical objects appear much brighter in the backscattered image, suggesting material that is higher in atomic number such as Ca and P.

EDS analysis of both nodule types show significantly higher Ca and P content than that of cells. For dystrophic nodules, however, the majority of the scans on the nodule revealed very low Ca and P values similar to those from cells. Regions that exhibited high Ca and P contents seemed to be embedded between the rounded surface structures and were giving information about the material deeper within the nodule. Chen et al. revealed through TEM imaging of a dystrophic nodule that the bulk calcification was found beneath a layer of cells covering the surface [27]. Because the interaction volume for both backscattered electrons and X-ray generation is limited to a few microns in depth and varies with atomic number, regions beneath the surface of an unpolished sample cannot be effectively characterized [35]. Taken together, our EDS data suggest that the dystrophic nodule surface is comprised mostly of cellular material, but there is evidence of Ca and P deeper within the nodule. Conversely, osteogenic nodules had abundant surface calcification. EDS confirmed that the spherical objects on the surface of osteogenic nodules were high in Ca and P concentrations. These novel findings are consistent with a recent EDS analysis of in vivo valve calcification that described the presence of spherical calcifications on the surface of valve tissue [28]. Additionally, the nodule body of osteogenic CNs contained higher levels of Ca and P than cells indicating the presence of embedded bone matrix characteristic of osteogenesis. Both nodule types exhibited Ca and P ratios consistent with hydroxyapatite with dystrophic nodules having a Ca and P ratio of 2.0 and osteogenic nodules having a Ca and P ratio of 1.67 [36]. Further, osteogenic calcifications had significantly higher amounts of Ca and P when compared to dystrophic calcification. These physicochemical similarities and differences could prove to be important hallmarks distinguishing between calcification types [37].

AFM data for dystrophic and osteogenic nodules complemented the SEM-EDS data. For dystrophic nodules, the scans showed a high level of topographical heterogeneity as evidenced by the change in height throughout scans. This is consistent with the bumpy morphology of the dystrophic nodule surface. The modulus data show approximately cellular stiffness throughout the majority of the scans supporting the notion that the dystrophic nodule surface is mostly cellular. For osteogenic nodules, height and modulus scans along the nodule body were mostly homogeneous with modulus readings in the range of cellular modulus. This suggests that although the osteogenic nodule body is high in Ca and P, it mostly comprised cells. This is consistent with the bone formation process, which has been described to contain osteogenic cells embedded in the bone matrix that they are secreting [38]. Further, regions containing spherical objects were also identified via AFM. These regions were dramatically stiffer than the nodule body and the cells, suggesting that they are noncellular material. The increased stiffness of these spheres support the EDS spectrum and backscattered SEM images of osteogenic nodules further suggesting that these spherical objects are calcified. The presence of regions exhibiting distinct properties in the osteogenic nodule highlights the heterogeneous make up of osteogenic CNs, which distinguishes it from dystrophic CNs.

This physicochemical and biophysical analysis of CNs provides new insight into dystrophic and osteogenic calcification. Our data demonstrate that dystrophic and osteogenic nodules exhibit different properties. Dystrophic nodules were found to exhibit a bumpy topography with a modulus similar to cells. Ca and P were found in regions that appeared to be deeper within the nodule suggesting that dystrophic CNs have mineralized content beneath the surface. Osteogenic nodules displayed nodule heterogeneity with regions rich in stiff calcified spheres and smooth regions comprised mostly of cells. Levels of Ca and P were elevated in both the nodule body and the calcified spheres. These findings demonstrate for the first time the unique physicochemical and biophysical characteristics of dystrophic and osteogenic CNs.

Future Work

Future work includes the characterization of these systems over multiple time points. In this work, the time points for analysis were chosen based upon the literature; however, one major limitation in the CN assays is ambiguity regarding nodule endpoints. A thorough characterization of CN formation over time could generate further insight into how dystrophic and osteogenic nodules mature. Additionally, other techniques may be implemented in the analysis of CNs. This study utilized primarily surface/subsurface techniques to analyze CNs. Although these techniques can comprehensively describe surface properties, they are limited in their ability to characterize the material properties beneath the surface. Tools such as TEM can be used to generate more information regarding the characteristics of CNs beneath the surface.

Acknowledgment

This work was supported by the NIH (Nos. HL094707 and HL115103) and NSF (No. 1055384), all awarded to W.D.M. J.C. was supported as a Pre-doctoral Fellow by the American Heart Association (No. 11PRE7990023).

References

[1] Otto, C. M., Kuusisto, J., Reichenbach, D. D., Gown, A. M., and O'brien, K. D., 1994, "Characterization of the Early Lesion of 'Degenerative' Valvular Aortic Stenosis. Histological and Immunohistochemical Studies," Circulation, **90**(2), pp. 844–853.

[2] Freeman, R. V., and Otto, C. M., 2005, "Spectrum of Calcific Aortic Valve Disease: Pathogenesis, Disease Progression, and Treatment Strategies," Circulation, **111**(24), pp. 3316–3326.

[3] Iung, B., and Vahanian, A., 2011, "Epidemiology of Valvular Heart Disease in the Adult," Nat. Rev. Cardiol., **8**(3), pp. 162–172.

[4] Dweck, M. R., Boon, N. A., and Newby, D. E., 2012, "Calcific Aortic Stenosis: A Disease of the Valve and the Myocardium," J. Am. Coll. Cardiol., **60**(19), pp. 1854–1863.

[5] Chen, J. H., and Simmons, C. A., 2011, "Cell-Matrix Interactions in the Pathobiology of Calcific Aortic Valve Disease: Critical Roles for Matricellular, Matricrine, and Matrix Mechanics Cues," Circ. Res., **108**(12), pp. 1510–1524.

[6] Mohler III, E. R., Gannon, F., Reynolds, C., Zimmerman, R., Keane, M. G., and Kaplan, F. S., 2001, "Bone Formation and Inflammation in Cardiac Valves," Circulation, **103**(11), pp. 1522–1528.

[7] Langanay, T., Flecher, E., Fouquet, O., Ruggieri, V. G., De La Tour, B., Felix, C., Lelong, B., Verhoye, J. P., Corbineau, H., and Leguerrier, A., 2012, "Aortic Valve Replacement in the Elderly: The Real Life," Ann. Thorac. Surg., **93**(1), pp. 70–77; Discussion 77–78.

[8] Thomas, M., Schymik, G., Walther, T., Himbert, D., Lefevre, T., Treede, H., Eggebrecht, H., Rubino, P., Michev, I., Lange, R., Anderson, W. N., and Wendler, O., 2010, "Thirty-Day Results of the Sapien Aortic Bioprosthesis European Outcome (Source) Registry: A European Registry of Transcatheter Aortic Valve Implantation Using the Edwards Sapien Valve," Circulation, **122**(1), pp. 62–69.

[9] Hutcheson, J. D., Aikawa, E., and Merryman, W. D., 2014, "Potential Drug Targets for Calcific Aortic Valve Disease," Nat. Rev. Cardiol., **11**(4), pp. 218–231.

[10] Hutcheson, J. D., Ryzhova, L. M., Setola, V., and Merryman, W. D., 2012, "5-Ht(2b) Antagonism Arrests Non-Canonical Tgf-Beta1-Induced Valvular Myofibroblast Differentiation," J. Mol. Cell. Cardiol., **53**(5), pp. 707–714.

[11] Yip, C. Y., Blaser, M. C., Mirzaei, Z., Zhong, X., and Simmons, C. A., 2011, "Inhibition of Pathological Differentiation of Valvular Interstitial Cells by C-Type Natriuretic Peptide," Arterioscler. Thromb. Vasc. Biol., **31**(8), pp. 1881–1889.

[12] Walker, G. A., Masters, K. S., Shah, D. N., Anseth, K. S., and Leinwand, L. A., 2004, "Valvular Myofibroblast Activation by Transforming Growth Factor-Beta: Implications for Pathological Extracellular Matrix Remodeling in Heart Valve Disease," Circ. Res., **95**(3), pp. 253–260.

[13] Yip, C. Y., Chen, J. H., Zhao, R., and Simmons, C. A., 2009, "Calcification by Valve Interstitial Cells is Regulated by the Stiffness of the Extracellular Matrix," Arterioscler. Thromb. Vasc. Biol., **29**(6), pp. 936–942.
[14] Jian, B., Narula, N., Li, Q. Y., Mohler III, E. R., and Levy, R. J., 2003, "Progression of Aortic Valve Stenosis: Tgf-Beta1 is Present in Calcified Aortic Valve Cusps and Promotes Aortic Valve Interstitial Cell Calcification Via Apoptosis," Ann. Thorac. Surg., **75**(2), pp. 457–465; Discussion 465–466.
[15] Benton, J. A., Kern, H. B., Leinwand, L. A., Mariner, P. D., and Anseth, K. S., 2009, "Statins Block Calcific Nodule Formation of Valvular Interstitial Cells by Inhibiting Alpha-Smooth Muscle Actin Expression," Arterioscler. Thromb. Vasc. Biol., **29**(11), pp. 1950–1957.
[16] Mohler III, E. R., Chawla, M. K., Chang, A. W., Vyavahare, N., Levy, R. J., Graham, L., and Gannon, F. H., 1999, "Identification and Characterization of Calcifying Valve Cells from Human and Canine Aortic Valves," J. Heart Valve Dis., **8**(3), pp. 254–260.
[17] Gu, X., and Masters, K. S., 2011, "Role of the Rho Pathway in Regulating Valvular Interstitial Cell Phenotype and Nodule Formation," Am. J. Physiol. Heart Circ. Physiol., **300**(2), pp. H448–H458.
[18] Gu, X., and Masters, K. S., 2009, "Role of the Mapk/Erk Pathway in Valvular Interstitial Cell Calcification," Am. J. Physiol. Heart Circ. Physiol., **296**(6), pp. H1748–H1757.
[19] Fisher, C. I., Chen, J., and Merryman, W. D., 2013, "Calcific Nodule Morphogenesis by Heart Valve Interstitial Cells Is Strain Dependent," Biomech. Model. Mechanobiol., **12**(1), pp. 5–17.
[20] Hutcheson, J. D., Chen, J., Sewell-Loftin, M. K., Ryzhova, L. M., Fisher, C. I., Su, Y. R., and Merryman, W. D., 2013, "Cadherin-11 Regulates Cell-Cell Tension Necessary for Calcific Nodule Formation by Valvular Myofibroblasts," Arterioscler. Thromb. Vasc. Biol., **33**(1), pp. 114–120.
[21] Bowler, M. A., and Merryman, W. D., 2015, "In Vitro Models of Aortic Valve Calcification: Solidifying a System," Cardiovasc. Pathol. **25**(1), pp. 1–10.
[22] Benton, J. A., Kern, H. B., and Anseth, K. S., 2008, "Substrate Properties Influence Calcification in Valvular Interstitial Cell Culture," J. Heart Valve Dis., **17**(6), pp. 689–699.
[23] Valente, M., Bortolotti, U., and Thiene, G., 1985, "Ultrastructural Substrates of Dystrophic Calcification in Porcine Bioprosthetic Valve Failure," Am. J. Pathol., **119**(1), pp. 12–21.
[24] Zhao, Y., Urganus, A. L., Spevak, L., Shrestha, S., Doty, S. B., Boskey, A. L., and Pachman, L. M., 2009, "Characterization of Dystrophic Calcification Induced in Mice by Cardiotoxin," Calcif. Tissue Int., **85**(3), pp. 267–275.
[25] Rajamannan, N. M., Subramaniam, M., Rickard, D., Stock, S. R., Donovan, J., Springett, M., Orszulak, T., Fullerton, D. A., Tajik, A. J., Bonow, R. O., and Spelsberg, T., 2003, "Human Aortic Valve Calcification is Associated With an Osteoblast Phenotype," Circulation, **107**(17), pp. 2181–2184.
[26] Cloyd, K. L., El-Hamamsy, I., Boonrungsiman, S., Hedegaard, M., Gentleman, E., Sarathchandra, P., Colazzo, F., Gentleman, M. M., Yacoub, M. H., Chester, A. H., and Stevens, M. M., 2012, "Characterization of Porcine Aortic Valvular Interstitial Cell 'Calcified' Nodules," PLoS One, **7**(10), p. e48154.
[27] Chen, J. H., Yip, C. Y., Sone, E. D., and Simmons, C. A., 2009, "Identification and Characterization of Aortic Valve Mesenchymal Progenitor Cells With Robust Osteogenic Calcification Potential," Am. J. Pathol., **174**(3), pp. 1109–1119.
[28] Bertazzo, S., Gentleman, E., Cloyd, K. L., Chester, A. H., Yacoub, M. H., and Stevens, M. M., 2013, "Nano-Analytical Electron Microscopy Reveals Fundamental Insights into Human Cardiovascular Tissue Calcification," Nat. Mater., **12**(6), pp. 576–583.
[29] Merryman, W. D., Liao, J., Parekh, A., Candiello, J. E., Lin, H., and Sacks, M. S., 2007, "Differences in Tissue-Remodeling Potential of Aortic and Pulmonary Heart Valve Interstitial Cells," Tissue Eng., **13**(9), pp. 2281–2289.
[30] Wang, H., Haeger, S. M., Kloxin, A. M., Leinwand, L. A., and Anseth, K. S., 2012, "Redirecting Valvular Myofibroblasts into Dormant Fibroblasts through Light-Mediated Reduction in Substrate Modulus," PLoS One, **7**(7), p. e39969.
[31] Engler, A. J., Sen, S., Sweeney, H. L., and Discher, D. E., 2006, "Matrix Elasticity Directs Stem Cell Lineage Specification," Cell, **126**(4), pp. 677–689.
[32] Tse, J. R., and Engler, A. J., 2010, "Preparation of Hydrogel Substrates With Tunable Mechanical Properties," Curr. Protoc. Cell. Biol. Chapter 10.
[33] Gregory, C. A., Gunn, W. G., Peister, A., and Prockop, D. J., 2004, "An Alizarin Red-Based Assay of Mineralization by Adherent Cells in Culture: Comparison With Cetylpyridinium Chloride Extraction," Anal. Biochem., **329**(1), pp. 77–84.
[34] Sewell-Loftin, M. K., Brown, C. B., Baldwin, H. S., and Merryman, W. D., 2012, "A Novel Technique for Quantifying Mouse Heart Valve Leaflet Stiffness With Atomic Force Microscopy," J. Heart Valve Dis., **21**(4), pp. 513–520.
[35] Goldstein, J., 2003, *Scanning Electron Microscopy and X-Ray Microanalysis*, Kluwer Academic/Plenum Publishers, New York.
[36] Bonucci, E., 2007, *Biological Calcification: Normal and Pathological Processes in the Early Stages*, Springer, Berlin New York.
[37] Benjamin Kramer, M. J. S., 1928, "Composition of Bone: Iv. Primary Calcification," J. Biol. Chem., **79**, pp. 147–160.
[38] Gilbert, S. F., 2000, *Developmental Biology*, Sinauer Associates, Sunderland, MA.